Analysis of pulsatile shear-thinning flows in rectangular channels

Nayeon Park and Jaewook Nam*
School of Chemical and Biological Engineering, Institute of Chemical Processes, Seoul National University, Seoul 08826, South Korea

(Received 9 June 2022; accepted 8 November 2022; published 1 December 2022)

In this paper, we present an in-depth analysis of pulsatile shear-thinning flows in two-dimensional channels. The characteristic viscosity was determined based on steady-state analysis of non-Newtonian flows and was used to nondimensionalize the flow system by introducing the non-Newtonian Womersley number. Numerical analyses on various Carreau fluids revealed the existence of master curves related to the amplitude and phase lag of the flows, where the shape of the master curve is determined by the degree of shear thinning. Such master curves imply that the competition between viscous and pulsatile time scales can be described appropriately by using the non-Newtonian Womersley number proposed in this paper. Furthermore, it is demonstrated that the flow dynamics can be predicted accurately using precomputed master curves, presenting a method for predicting shear-thinning pulsatile flow dynamics without explicit transient computations.

DOI: 10.1103/PhysRevFluids.7.123301

I. INTRODUCTION

Various external disturbances, such as oscillations from flow pumps or vibrations from machine frames, are commonly encountered in chemical processes when solutions are transported through a series of pipe systems. For example, the frequency and magnitude ranges of industrial slot coating processes have been presented [1]. The solution transport process is important for the production of high value-added products, such as batteries and flexible displays. The performance of these products may be significantly affected by changes in the rheological properties or microstructure of complex non-Newtonian fluids induced by unpredictable disturbances. Therefore, it is necessary to gain an in-depth understanding of time-dependent non-Newtonian flows.

Among complex fluids, this paper focused on slurries, which can be considered as a mixture of dense particles suspended in a solution. Typical industrial slurries, such as cement, coal, and battery slurries, are high-concentration suspensions. These slurries exhibit strong non-Newtonian behavior characterized by yield stress, viscoelastic, thixotropic, and shear-thinning behaviors [2–6]. In this paper, the effect of shear thinning was investigated under transient conditions.

Flows with periodic disturbances, that is, pulsatile flows, have been a topic of interest for several decades, and numerous experimental and theoretical studies on pulsatile Newtonian flows have been conducted [7–10]. Particularly, an analytical solution for arbitrary pulsating pressure gradients was derived using dimensionless parameters [10]. For non-Newtonian fluids, the oscillatory behavior of blood flow has been studied exclusively using various models, such as the power-law, Cross, Carreau, and Carreau-Yasuda models [11–14]. Additionally, a number of studies have investigated the flow enhancements of non-Newtonian pulsatile flows [15–19].

To date, in-depth analyses of pulsatile non-Newtonian systems have been scarce, as most studies have focused on reporting pressure gradients, velocity, and stress profiles, or have treated the system

*jaewooknam@snu.ac.kr

using simplified governing equations under limited conditions through asymptotic analysis [14]. Therefore, in this paper, we revisit the classical pulsatile shear-thinning flow problem and interpret it from a different perspective.

In this paper, the characteristic viscosity of pulsatile shear-thinning flow was defined and used to form the non-Newtonian Womersley number, which acts as a key model parameter of the system of interest. Numerical experiments were conducted using Carreau fluids with various rheological parameters and frequencies to analyze the effect of each parameter on flow behavior. Master curves were revealed by plotting the nondimensionalized numerical results with respect to the non-Newtonian Womersley number. Finally, a method was proposed to predict pulsatile flow dynamics using master curves without explicit transient computations.

II. PROBLEM FORMULATION

The constitutive equation relating the stress tensor to the strain-rate tensor must be specified to describe a viscous fluid in motion. Generalized non-Newtonian models are commonly used for shear-thinning fluids, of which we chose to use the Carreau model in this paper. The constitutive equation of the Carreau model is expressed as follows:

$$\eta(\dot{\gamma}) = \eta_\infty + (\eta_0 - \eta_\infty)[1 + (\lambda\dot{\gamma})^2]^{(n-1)/2}, \tag{1}$$

where η is the viscosity, $\dot{\gamma}$ is the shear rate, and η_0, η_∞, λ, and n are the model parameters.

Although constant viscosity can characterize a Newtonian fluid, selecting a single viscosity to represent a non-Newtonian flow is challenging because the flow has varying local viscosities depending on the local shear rates. Therefore, it is worthwhile to establish a reasonable methodology for determining the physical quantity of a non-Newtonian flow corresponding to the viscosity of Newtonian flow, which indicates the magnitude of the fluid's resistance to deformation. In this paper, this quantity is referred to as the characteristic viscosity.

A. Characteristic viscosity

We define the characteristic viscosity as the viscosity of a Newtonian fluid that yields the same pressure drop as non-Newtonian flow. By applying the Weissenberg-Rabinowitsch-Mooney-Schofield (WRMS) method, a direct integral relationship between the flow rate and the wall shear stress can be obtained [20–22]. Then, the Poiseuille equation can be used to relate the pressure drop of Newtonian flow to that of non-Newtonian flow.

A generalized Newtonian fluid flowing through a two-dimensional rectangular channel with height $2H$ was considered. When the flow is assumed to be laminar, isothermal, incompressible, and fully developed, ignoring entrance and end effects, the integral relationship can be derived using the WRMS method, as follows:

$$q = \frac{2H^2}{\tau_w^2}\int_0^{\tau_w} \dot{\gamma}\tau \, d\tau, \tag{2}$$

where q, τ, and τ_w are the flow rate per unit width, shear stress, and wall shear stress, respectively. For constitutive equations wherein $\dot{\gamma}\tau^2$ is analytically integrable, such as Carreau and Cross fluids, q can be expressed in terms of τ_w in explicit form [21]. In other cases, numerical integration must be carried out.

The analog of the Poiseuille equation for Newtonian channel flow with viscosity μ can be expressed as follows:

$$-\frac{dp}{dx} = \frac{3\mu q}{2H^3}. \tag{3}$$

Then, using the characteristic viscosity η_N, the above equation can be expressed as follows:

$$-\frac{dp}{dx} = \frac{3\eta_N q}{2H^3}. \tag{4}$$

Next, Eq. (4) is related to the expression

$$\tau(y) = -y\frac{dp}{dx}, \tag{5}$$

and η_N can finally be written as follows:

$$\eta_N = \frac{2H^2\tau_w}{3q}. \tag{6}$$

Since τ_w can be computed using Eq. (2), η_N can be easily obtained without solving the partial differential equation (for example, the Navier-Stokes equation) governing the system.

B. Governing equations and dimensional analysis

The system of interest was the sinusoidal pulsatile channel flow of an incompressible non-Newtonian fluid under negligible body forces. A rectangular two-dimensional parallel channel has a height of $2H$ in the y direction and is considered sufficiently long to assume a fully developed parallel flow in the x direction. The flow should satisfy the mass balance equation

$$\nabla \cdot \mathbf{u} = 0 \tag{7}$$

and the momentum balance equation

$$\rho\left(\frac{\partial \mathbf{u}}{\partial t} + \mathbf{u}\cdot\nabla\mathbf{u}\right) = -\nabla p + \nabla\cdot\boldsymbol{\tau}\ , \tag{8}$$

where ρ is the density of the fluid, $\mathbf{u}$ is the velocity vector, p is the pressure, and $\boldsymbol{\tau}$ is the viscous stress tensor defined as follows:

$$\boldsymbol{\tau}\ = 2\eta(\dot{\gamma})\boldsymbol{E}\ , \tag{9}$$

where $\boldsymbol{E}\ = [\nabla\mathbf{u} + (\nabla\mathbf{u})^T]/2$ is the strain-rate tensor. The shear rate is given by $\dot{\gamma} = \sqrt{2\boldsymbol{E}\ :\boldsymbol{E}}$. Under the fully developed condition, Eqs. (7) and (8) can be reduced, respectively, as follows:

$$\frac{\partial u}{\partial x} = 0, \tag{10}$$

$$\frac{\partial u}{\partial t} = -\frac{1}{\rho}\frac{\partial p}{\partial x} + \frac{\eta}{\rho}\frac{\partial^2 u}{\partial y^2}, \tag{11}$$

where u is the x component of the velocity vector $\mathbf{u}$.

Let us examine pressure-driven pulsatile flow, where the time-dependent sinusoidal pressure gradient with frequency f is specified as follows:

$$-\frac{1}{\rho}\frac{\partial p}{\partial x} = p_0 + p_A \sin 2\pi f t, \tag{12}$$

where p_0 and p_A are the steady and oscillatory components of the pressure gradient, respectively.

To nondimensionalize the governing equation, characteristic time t_c and characteristic pressure $(-\frac{1}{\rho}\frac{\partial p}{\partial x})_c$ are defined as follows:

$$t_c = \frac{\rho H^2}{\eta_N}, \tag{13}$$

$$\left(-\frac{1}{\rho}\frac{\partial p}{\partial x}\right)_c = \frac{\eta_N u_{\text{avg}}}{\rho H^2}, \tag{14}$$

where u_{avg} is the average velocity in space when the flow is considered to be a Newtonian fluid with viscosity η_N. Notably, although the current system of interest exhibits time-dependent behavior, our choice of characteristic viscosity is deduced from *steady-state analysis*, as discussed in the previous section. For a given steady pressure gradient, p_0, the corresponding u_{avg} can be expressed as

$$u_{\text{avg}} = p_0 \frac{\rho H^2}{3\eta_N}, \tag{15}$$

which leads to the following alternative expression for Eq. (14):

$$\left(-\frac{1}{\rho}\frac{\partial p}{\partial x}\right)_c = \frac{p_0}{3}. \tag{16}$$

The dimensionless variables are defined in the same manner as in a previous study [10], as

$$y^* = \frac{y}{H}, \tag{17}$$

$$u^* = \frac{u}{u_{\text{avg}}}, \tag{18}$$

$$p^* = \frac{p}{p_0}, \tag{19}$$

$$T = \frac{t}{t_c}, \tag{20}$$

$$F = f t_c, \tag{21}$$

and can be used to nondimensionalize Eq. (11) as follows:

$$\frac{\partial u^*}{\partial T} = \left(-\frac{1}{\rho}\frac{\partial p}{\partial x}\right)^* + \frac{\partial^2 u^*}{\partial y^{*2}}. \tag{22}$$

The prescribed pulsatile pressure gradient expressed by Eq. (12) can also be nondimensionalized using Eq. (16) as follows:

$$\left(-\frac{1}{\rho}\frac{\partial p}{\partial x}\right)^* = 3(1 + p_A^* \sin 2\pi F T), \tag{23}$$

where p_A^* is the dimensionless form of p_A, that is, $p_A^* = p_A/p_0$. Then, Eq. (23) can be normalized as follows:

$$\nabla\hat{P} = \frac{1}{3}\left(-\frac{1}{\rho}\frac{\partial p}{\partial x}\right)^* = 1 + p_A^* \sin 2\pi F T, \tag{24}$$

such that the steady part can be set to 1.

The Womersley number α is a dimensionless number governing the flow characteristics of pulsatile Newtonian flow, and is defined as follows:

$$\alpha = R\left(\frac{2\pi f \rho}{\mu}\right)^{\frac{1}{2}}, \tag{25}$$

where R is the characteristic length, that is, $R = H$ in this paper, and f is the pulsation frequency [23]. This equation relates the transient inertial force to the viscous force. Using α, pulsatile flows can be categorized into three different regimes, namely, the quasisteady ($\alpha < 1.32$), intermediate ($1.32 < \alpha < 28$), and inertia-dominant ($\alpha > 28$) regimes [24]. When the geometry (R) and material parameters (ρ, μ) are fixed, α is the sole function of f and can be expressed using the dimensionless frequency F as $\alpha = (2\pi F)^{\frac{1}{2}}$.

This paper extends the definition of the Womersley number of a non-Newtonian fluid by adopting the above-mentioned characteristic viscosity. The Womersley number of a non-Newtonian pulsatile flow with frequency f and characteristic viscosity η_N is defined as

$$\alpha_N \equiv R\left(\frac{2\pi f \rho}{\eta_N}\right)^{\frac{1}{2}}. \tag{26}$$

This Womersley number plays an essential role in the dimensional analysis of non-Newtonian pulsatile flows and was used throughout this paper.

C. Flow regimes of pulsatile shear-thinning flows

Flow regimes of oscillatory Carreau flows have been separated according to the Womersley number and the Carreau number ($\Lambda \equiv \lambda u_{\text{avg}}/2H$) in [14]. Although the system in [14] is similar to ours, some differences exist; we are interested in a pulsatile mass-driven flow with base flow contribution, whereas the authors of [14] considered pressure gradient-driven flows oscillating from a stationary state. Owing to the similarities between the systems, we adopted the classification of flow regimes to shed light on how our system behaves under certain conditions, including limiting behaviors.

Following the mathematical arguments presented in [14], one can obtain asymptotic expansions in α_N^2 in the quasisteady regime where $\alpha_N \ll 1$ and in $1/\alpha_N^2$ in the inertia-dominant regime where $\alpha_N \gg 1$. Furthermore, when Λ is small enough, asymptotic expansions can be developed in Λ^2. In these regimes, solutions can be analyzed by using asymptotic methods, but as we will discuss in the following paragraphs such regimes do not cover the parameter range of interest. We are interested in intermediate α_Ns and non-negligible Λs, where the solutions must be obtained numerically.

Some of the limiting behaviors can be directly anticipated from the flow curves. The shear-thinning behavior of Carreau fluids mainly arises from parameters λ and n. We thereby classified flow curves of the Carreau fluid as in Fig. 1. If $\lambda \to 0$, the shear-thinning behavior is exhibited in a high-shear rate regime, which is beyond the effective shear rate region of interest such that the flow can be considered Newtonian, whereas, if $\lambda \to \infty$, the Carreau fluid approaches the power-law fluid because shear-thinning behavior starts in a low-shear rate regime. When n approaches unity, the degree of shear thinning, that is, the slope of the flow curve, is negligible, resulting in the fluid behaving as Newtonian fluid.

The λ and n values of typical industrial shear-thinning fluids (e.g., battery slurries) fall in the range $0.1 < \lambda < 100$ s and $0.4 < n < 0.7$, and the frequency ranges from 0.1 to 100 Hz. These values correspond to the regime where fluid cannot be simplified to a power-law or Newtonian fluid, and where a numerical solution is inevitable. Therefore, we focus on gaining insights into flows in transitional regimes with the aid of numerical methods.

D. Pulsatile pressure gradient-driven versus mass flow-driven flow

In this section, the relationship between the pulsatile pressure gradient-driven and the mass flow-driven flow is clarified. For Newtonian fluids, an analytic solution of the pulsatile pressure-driven flow described in the previous section exists for the mass flow $\dot{m}$ [10] as

$$\dot{m} = \dot{m}_0 + \dot{m}_A \sin{(2\pi f t - \Delta\theta_m)}, \tag{27}$$

where $\dot{m}_0$ and $\dot{m}_A$ are the steady and oscillatory components of the pressure gradient, respectively, and $\Delta\theta_m$ is the phase lag between the mass flow rate and the pressure gradient. Equation (27) can be scaled with $\dot{m}_0$ to be expressed in dimensionless form as

$$\dot{m}^* = 1 + \dot{m}_A^* \sin{(2\pi F T - \Delta\theta_m)}, \tag{28}$$

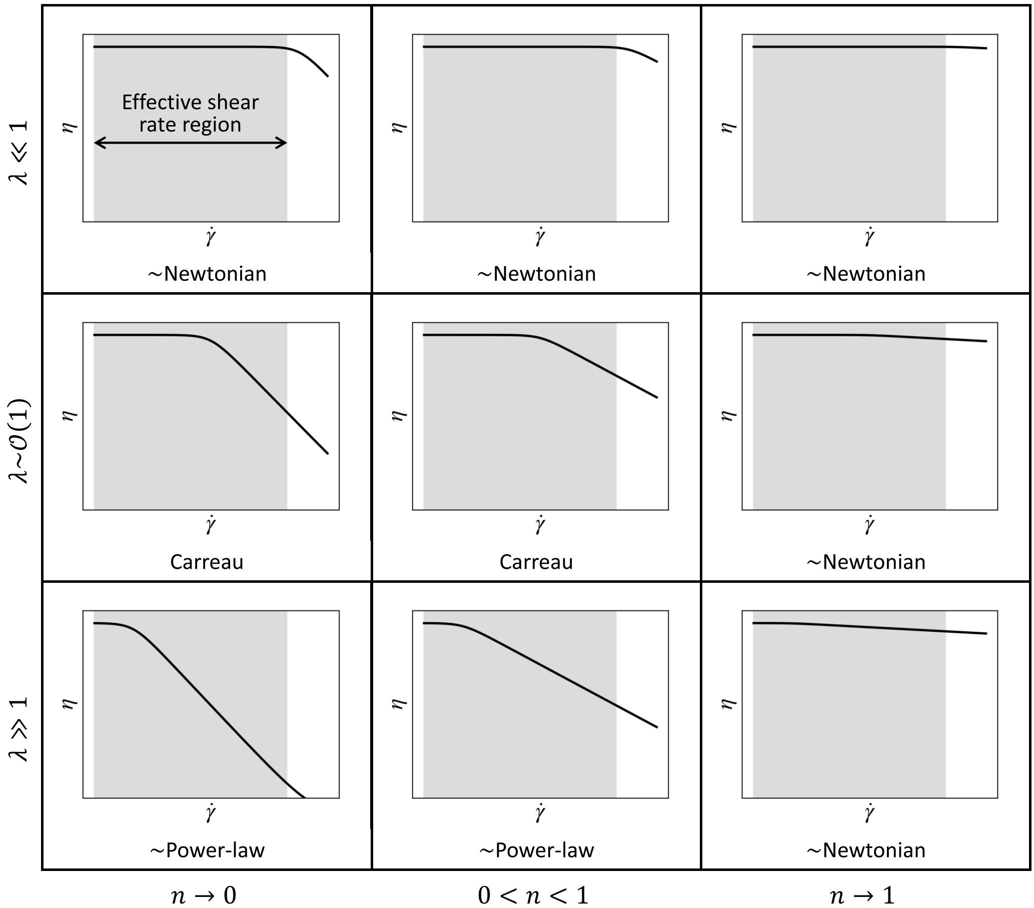

FIG. 1. Classification of Carreau flow curves according to λ and n values. The shear rate range of interest ($0 \leqslant \dot{\gamma} \leqslant \dot{\gamma}_w$) is highlighted in gray in the plot.

where $\dot{m}_A^*$ and $\Delta\theta_m$ can be expressed in terms of known parameters as

$$\dot{m}_A^* = p_A^* |\psi|, \tag{29}$$

$$\Delta\theta_m = -\arg\psi - \frac{\pi}{2}, \tag{30}$$

with parameter ψ defined as

$$\psi = -\frac{3}{\alpha^2}\left\{\frac{i^{\frac{1}{2}} J_{\frac{1}{2}}\left(\alpha i^{\frac{3}{2}}\right)}{\alpha J_{-\frac{1}{2}}\left(\alpha i^{\frac{3}{2}}\right)} + 1\right\}. \tag{31}$$

According to [8], for Newtonian fluids, the pulsatile pressure gradient and mass flow rate may be expressed as functions of one another, and knowledge of either of these suffices to determine all other unknowns of the flow. In other words, if the mass flow rate is imposed as

$$\dot{m}^* = 1 + \dot{m}_A^* \sin 2\pi F T \tag{32}$$

the resulting pressure gradient becomes

$$\nabla\hat{P} = 1 + p_A^* \sin\left(2\pi F T + \Delta\theta_m\right), \tag{33}$$

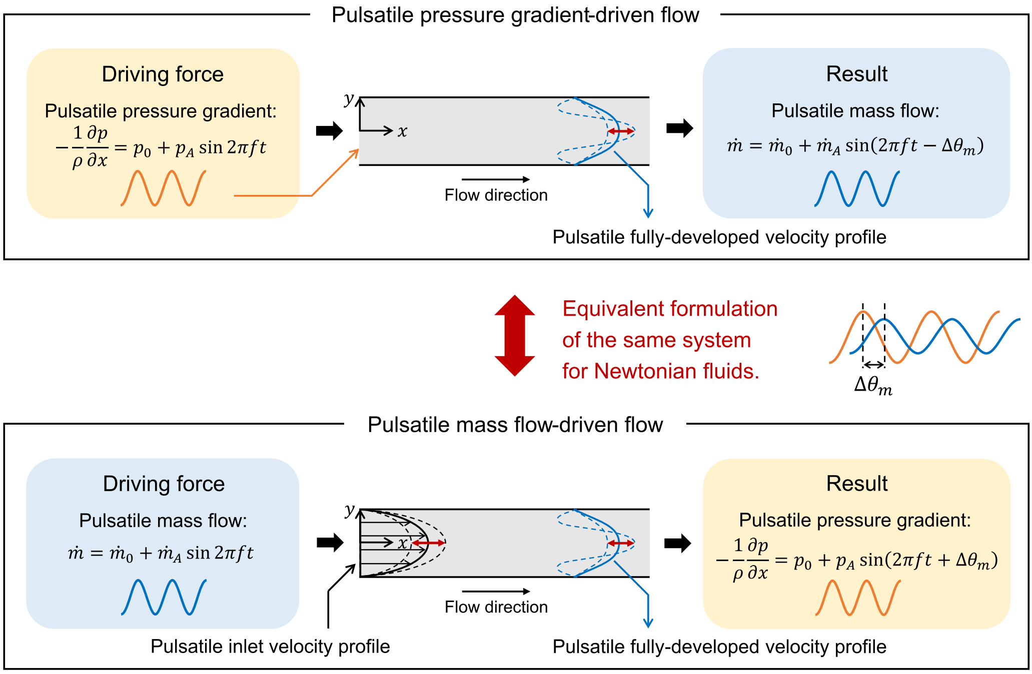

FIG. 2. Schematic of the relationship between pulsatile pressure gradient-driven and mass flow-driven flows. The equivalence of the two systems holds for Newtonian fluids.

with the same $\Delta\theta_m$ as in Eq. (30). A schematic summarizing of this relationship is presented in Fig. 2.

In this paper, we targeted pulsatile generalized Newtonian, particularly shear-thinning, flows under periodic *mass flow rate fluctuations*, which can model pulsating flows in industrial applications induced by positive displacement pumps, for example, diaphragm or gear pumps. To do so, we postulated that the pulsatile mass flow rate and consequent pressure gradient have the same frequency as the phase lag as in pulsatile Newtonian flows, implying that pressure and flow oscillations can be interchanged via a phase difference. The validity of our postulation is demonstrated numerically in the following sections.

III. NUMERICAL ANALYSIS

This section discusses the numerical methods and boundary conditions used in the computation and parameter setup of the numerical experiments. The in-house code was developed in the PYTHON language using FEniCS, which is an open-source computing platform for solving partial differential equations (PDEs) [25,26].

A. Numerical methods

The solution was computed using the method of lines approach, which is a numerical technique for solving time-dependent PDEs by discretizing the derivatives to reduce the problem to a system of ordinary differential equations (ODEs). The resulting ODEs can be integrated through various numerical schemes to obtain a solution. In this paper, the finite element method was used for spatial discretization, and the trapezoid rule with finite difference interrupts was used for time integration [27].

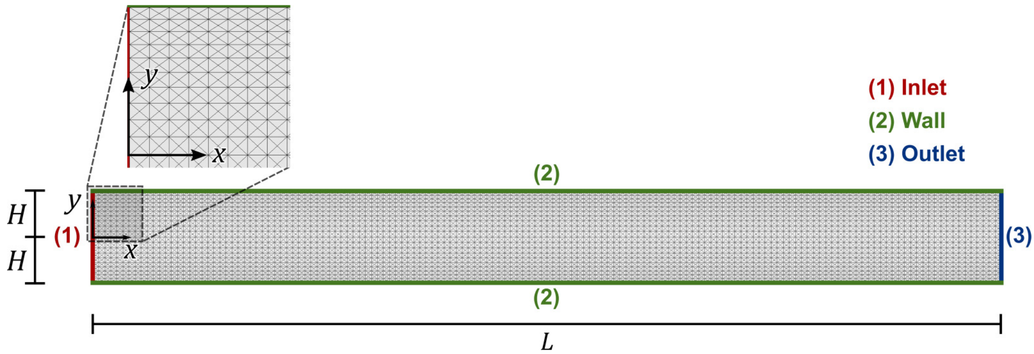

FIG. 3. Mesh configuration of two-dimensional channel where $H = 25$ mm and $L = 500$ mm. The computational domain was discretized by 12 000 triangular elements. The inlet, wall, and outlet boundary conditions are labeled with numbers.

With a proper choice of the basis functions for velocity and pressure, a variational form of the governing equations expressed by Eqs. (7) and (8) can be constructed as follows:

$$\int_{\Omega} \rho \frac{\partial \mathbf{u}}{\partial t} \cdot \mathbf{v}\, d\Omega + \int_{\Omega} \rho(\mathbf{u} \cdot \nabla \mathbf{u}) \cdot \mathbf{v}\, d\Omega + \int_{\Omega} \boldsymbol{\sigma} : \boldsymbol{E}(\mathbf{v})\, d\Omega$$
$$- \int_{\partial\Omega} [2\eta(\mathbf{u})\boldsymbol{E}(\mathbf{u}) \cdot \mathbf{n}] \cdot \mathbf{v}\, d\partial\Omega + \int_{\Omega} (\nabla \cdot \mathbf{u}) \cdot q\, d\Omega = 0, \tag{34}$$

where $\boldsymbol{\sigma} = 2\eta(\mathbf{u})\boldsymbol{E}(\mathbf{u}) - p\boldsymbol{I}$ is the total stress tensor, and $\mathbf{v}$ and q are the test functions of $\mathbf{u}$ and p, respectively. For viscous incompressible fluids, the mixed finite elements must satisfy the Ladyzhenskaya-Babuska-Brezzi (LBB) condition to achieve accurate and stable solutions [28,29]. In this paper, the P_2P_1 element (quadratic velocity field and linear pressure field), which is known to be LBB stable for triangular elements [30], was used.

The trapezoidal rule with finite difference interrupts is a time integration method that removes the recursion of the trapezoidal derivative by replacing it with the backward finite difference formula [27]. In this paper, a finite difference interrupt was applied with the interval of two time steps, and the second-order Adams-Bashforth formula was used as the predictor.

B. Computational domain with initial and boundary conditions

The mesh configuration of the two-dimensional channel considered in the computations is shown in Fig. 3. The channel was sufficiently long ($L \gg H$) to ensure a fully developed parallel flow in the x direction [31]. Triangular elements were used, and the elements were more finely spaced near the wall to capture strong velocity gradients. A no-slip boundary condition was specified at the walls and a pulsatile velocity condition was specified at the inlet. The outlet pressure was set to zero.

In this paper, we numerically solved for the two-dimensional pulsatile flow of shear-thinning fluids under periodic mass flow rate fluctuations. If the system was a fully developed parallel flow under a pulsatile pressure gradient, it could be simplified to a one-dimensional model by solving Eq. (11) with a time-dependent pressure gradient as a source term. However, as our system is pulsatile mass flow driven, a time-dependent velocity profile must be provided as an inlet boundary condition to solve the problem, complicating the issue. Contrary to Newtonian flows, where a fully developed velocity profile is parabolic, obtaining a fully developed *a priori* velocity profile for non-Newtonian flows is difficult, if not impossible. Consequently, the problem was approached numerically to compute the flow developed along the x direction of the two-dimensional channel.

Without knowledge of the fully developed velocity profile, we chose the Newtonian velocity profile, that is, a parabolic profile, as an inlet boundary condition because it satisfies the no-slip

TABLE I. Carreau parameters of model fluid and corresponding wall shear rate, characteristic viscosity, and pressure gradient computed through steady-state analysis using the WRMS method.

	Carreau parameters				Computed values		
Case	η_0 (Pa s)	η_∞ (Pa s)	λ (s)	n	$\dot{\gamma}_w$ (s^{-1})	η_N (Pa s)	$-dp/dx$ (kPa/m)
Base	**50**	**0.01**	**1**	**0.5**	108.5	6.404	6.63
1	**25**	0.01	1	0.5	108.4	3.207	10.45
2	**100**	0.01	1	0.5	108.6	12.80	41.72
3	**200**	0.01	1	0.5	108.6	25.59	83.40
4	50	0.01	**0.1**	0.5	106.7	20.01	65.21
5	50	0.01	**10**	0.5	108.5	2.033	6.626
6	50	0.01	**100**	0.5	107.8	0.6501	2.119
7	50	0.01	1	**0.4**	121.9	4.204	13.70
8	50	0.01	1	**0.6**	99.54	9.708	31.64
9	50	0.01	1	**0.7**	93.11	14.67	47.81

boundary condition and the exact flow rate, as shown in Eq. (32). Because the second-order basis function was used for the velocity field, the flow rate can be induced from the parabolic velocity profile without loss of information, thereby minimizing the approximation error originating from the numerical method. Accordingly, the parabolic inlet velocity profile was sinusoidally specified as

$$u(y) = u_{\max}\left(1+\frac{y}{H}\right)\left(1-\frac{y}{H}\right)(1+\dot{m}_A^* \sin 2\pi f t), \tag{35}$$

where $u_{\max}$ is the maximum velocity of the steady-state flow with the average flow rate as follows:

$$u_{\max} = \frac{3q}{4H}. \tag{36}$$

Here, $u_{\max} = 1.02\ \mathrm{ms}^{-1}$ corresponding to a flow rate of $1\ \mathrm{Ls}^{-1}$ was used. The amplitude was fixed at $\dot{m}_A^* = 0.1$.

C. Numerical experiments

1. Viscosity modeling

The Carreau model was used to describe the viscosity of a shear-thinning non-Newtonian fluid. Based on the authors' experience, the Carreau parameters were selected such that the viscosity of the base case would be comparable to that of typical battery slurries. Then, parameters η_0, λ, and n were varied to establish nine different test cases, as presented in Table I. The corresponding viscosity curves are shown in Fig. 4.

In this paper, we aimed to assess the effect of the Womersley number, α_N, on the flow characteristics, that is, to observe how the pressure gradient fluctuations behave under flow-rate disturbances. Since α_N is a function of the steady-state characteristic viscosity, η_N, parameters covering a wide range of η_N were selected.

2. Frequency range and Womersley number

Seven different frequencies in the range of 0.1–100 Hz were investigated to cover a wide range of frequencies that may occur during solution transportation. The Womersley numbers corresponding to different cases and frequencies are listed in Table II, where it can be observed that the range of Womersley numbers covers the quasisteady, intermediate, and inertia-dominant regimes, according to the criteria of Newtonian flow.

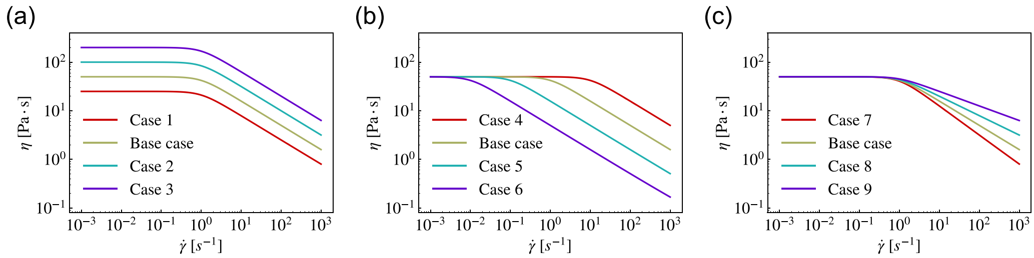

FIG. 4. Viscosity curves for test cases of Carreau model fluids when (a) η_0 is varied, (b) λ is varied, and (c) n is varied.

D. Validation of numerical method

We proved that our numerical solution of a pulsatile Newtonian flow is in good agreement with the analytic solution. The dimensionless time-dependent velocity profiles and pressure gradients were compared with analytic solutions of [10]. The velocity profiles at different times and sinusoidal pressure gradients were accurately predicted by numerical simulations, validating our numerical method for pulsatile Newtonian flows (see the Supplemental Material [32]).

To verify our method for pulsatile non-Newtonian flows, grid sensitivity analysis was performed for the velocity profile and the pressure gradient. Here, we demonstrate two extreme cases where the Womersley number is minimum (case 3, $f = 0.1$ Hz) and maximum (case 6, $f = 100$ Hz) among the test cases presented in the previous section. The pressure gradient was studied with the parameters p_A^* and $\Delta\theta_m$, which are critical in representing the pulsatile pressure gradient, as shown in Fig. 5. From the results, we concluded that grid independence is achieved, and our choice of 12 000 elements is reasonable, considering the accuracy and the efficiency of the computation at the same time.

IV. RESULTS AND DISCUSSION

This section discusses the analysis of the pressure gradients of the computed numerical solutions to compare the effects of changing each parameter (η_0, λ, and n). Moreover, a method for predicting the pulsatile flow dynamics using the master curves is introduced.

TABLE II. Womersley number (α_N) calculated for each case and frequency.

	Frequency (Hz)						
Case	0.1	0.3	1	3	10	30	100
Base	0.3033	0.5253	0.9591	1.661	3.033	5.253	9.591
1	0.4286	0.7424	1.355	2.348	4.286	7.424	13.55
2	0.2145	0.3716	0.6784	1.175	2.145	3.716	6.784
3	0.1517	0.2628	0.4798	0.8310	1.518	2.628	4.798
4	0.1716	0.2972	0.5426	0.9398	1.716	2.972	5.426
5	0.5383	0.9324	1.702	2.948	5.383	9.324	17.02
6	0.9519	1.649	3.010	5.214	9.519	16.49	30.10
7	0.3743	0.6483	1.184	2.050	3.743	6.483	11.84
8	0.2463	0.4266	0.7789	1.349	2.463	4.266	7.789
9	0.2004	0.3471	0.6337	1.098	2.004	3.471	6.337

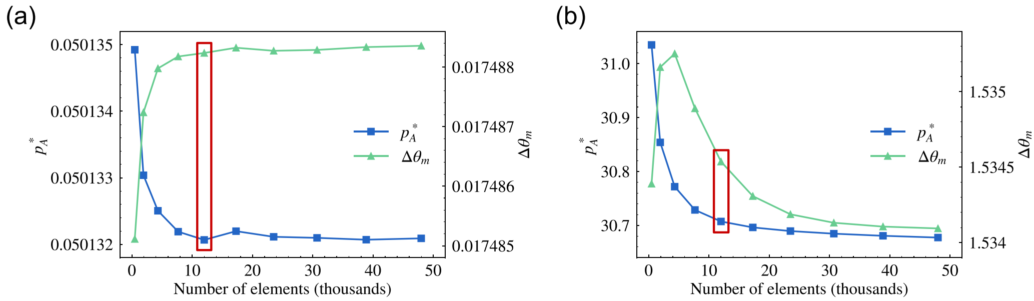

FIG. 5. Grid sensitivity study for (a) case 3 and (b) case 6. A mesh with 12 000 elements was chosen.

A. Pressure gradient fitting

The computed pressure gradients of the fully developed flows were nondimensionalized and normalized with a steady part, as follows:

$$\nabla\hat{P} = \frac{1}{3}\left(-\frac{1}{\rho}\frac{\partial p}{\partial x}\right)_n \Bigg/ \left(-\frac{1}{\rho}\frac{\partial p}{\partial x}\right)_c, \tag{37}$$

where $(-\frac{1}{\rho}\frac{\partial p}{\partial x})_n$ and $(-\frac{1}{\rho}\frac{\partial p}{\partial x})_c$ are the numerical solution and the characteristic pressure defined in Eq. (14), respectively. The normalized dimensionless pressure gradient was then fitted to Eq. (33). All pressure gradient results were well fitted, implying that the interchangeability between flow rate-driven and pressure-driven pulsatile flow formulations under the phase lag postulated in the previous section is valid. For example, Fig. 6 shows the fitted curves of the pressure gradient for the base case.

Here, we want to compare the non-Newtonian and Newtonian pressure gradients. Therefore, the amplification factor of the pressure gradient A_p is defined as follows:

$$A_p = \frac{p_A^*}{p_{A,\mathrm{Newtonian}}^*}, \tag{38}$$

where p_A^* and $p_{A,\mathrm{Newtonian}}^*$ are the amplitudes of the pressure gradient of a non-Newtonian fluid and Newtonian fluid with the characteristic viscosity of non-Newtonian flow, respectively; p_A^* was obtained from the numerical solution using Eq. (33) and $p_{A,\mathrm{Newtonian}}^*$ was determined by analytical solution [10]. In the following sections, A_p and $\Delta\theta_m$ will be discussed in detail.

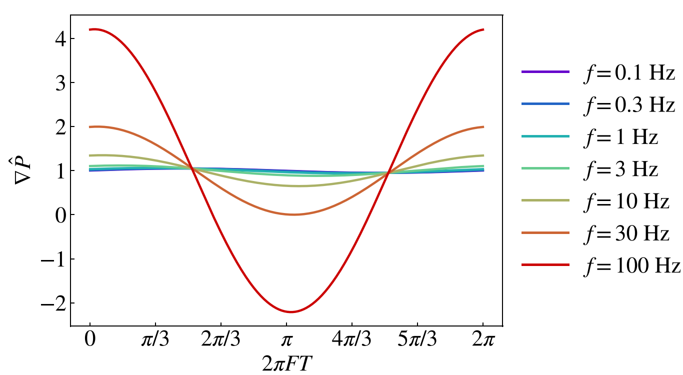

FIG. 6. Normalized pressure gradients of base case fitted to sinusoidal curve for $f = 0.1, 0.3, 1, 3, 10, 30,$ and 100 Hz.

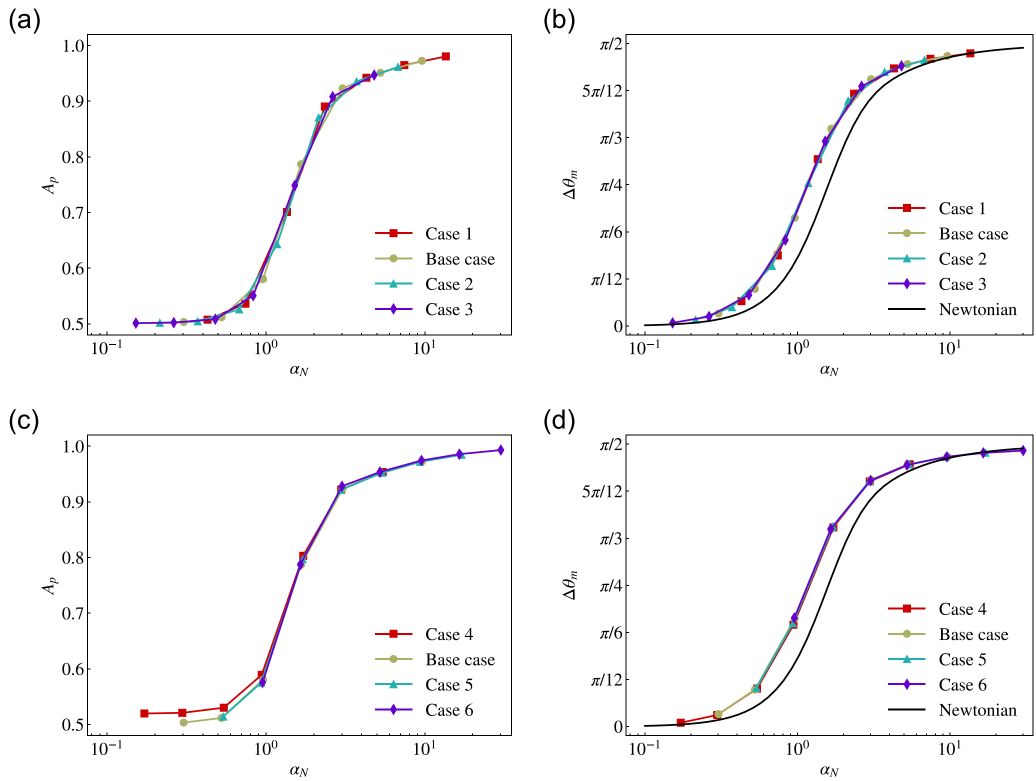

FIG. 7. (a) Amplification factor of pressure gradient and (b) phase lag between mass flow rate and pressure gradient with varying η_0 values; case 1, base case, case 2, and case 3 correspond to $\eta_0 = 25$, 50, 100, and 200, respectively. (c) Amplification factor of pressure gradient and (d) phase lag between mass flow rate and pressure gradient with varying λ values; case 1, base case, case 2, and case 3 correspond to $\lambda = 0.1$, 1, 10, and 100, respectively. The Newtonian solid lines in (b) and (d) indicate the phase lags of the Newtonian pulsatile flows with the corresponding Womersley number, α, calculated by the Newtonian analytic solution.

B. Effect of η_0 and λ

Figure 7(a) shows the amplification factor of pressure gradient A_p under differentη_0 values. The pulsation of the non-Newtonian pressure gradient is damped compared with the Newtonian one when α_N is low, but pressure gradient damping does not occur in the inertia-dominant regime, as demonstrated by A_p converging to unity as α_N increases.

In Fig. 7(b), the phase lag between the mass flow rate and the pressure gradient $\Delta\theta_m$ is compared to the Newtonian phase lag obtained by the analytical solution. The phase lag becomes more pronounced as the inertial effects become dominant at high Womersley numbers, where the flow cannot be in phase with the change in the pulsating inlet mass flow. As shown in Figs. 7(c) and 7(d), the effect of λ is similar to that of η_0; A_p converges to unity as α_N and $\Delta\theta_m$ increase, which indicates the dominance of inertial effects at high α_N.

From the existence of the single master curves of the amplification factors and phase lags of different model parameters, it is concluded that our definition of the Womersley number is appropriate for concisely representing the transient dynamics of non-Newtonian flows. Furthermore, the definition of characteristic viscosity appears to be suitable to shear-thinning fluids.

C. Effect of n

Parameter n is a measure of the degree of the shear-thinning behavior of a fluid; $n = 1$ indicates Newtonian behavior, and as n decreases below 1 the shear-thinning behavior becomes more

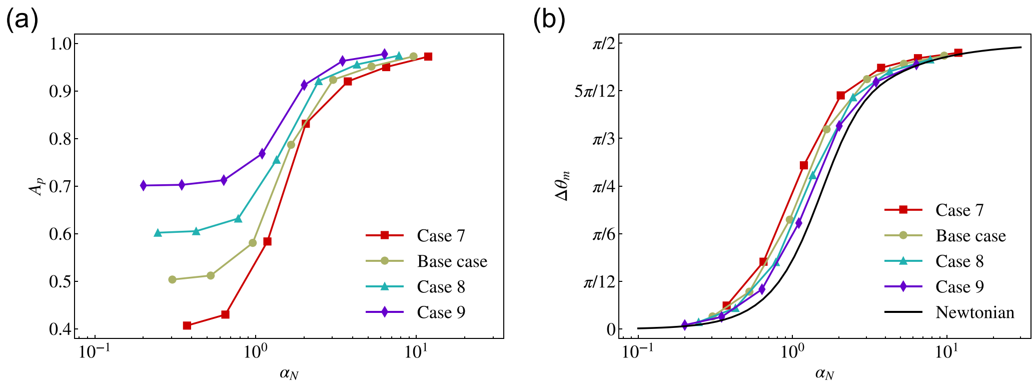

FIG. 8. (a) Amplification factor of pressure gradient and (b) phase lag between mass flow rate and pressure gradient with varying n values; case 7, base case, case 8, and case 9 correspond to $n = 0.5$, 0.6, 0.7, and 0.8, respectively. The Newtonian solid line in (b) indicates the phase lag of the Newtonian pulsatile flow with the corresponding Womersley number, α, calculated by the Newtonian analytic solution.

pronounced. When n is varied, A_p and $\Delta\theta_m$ exhibit different patterns compared with when η_0 or λ is varied. From Fig. 8(a), it is clear that A_p increases, that is, the pressure gradient is less damped at low α_N as n increases. Let us recall that A_p is the relative amplitude of the non-Newtonian pressure gradient compared to that of a Newtonian fluid. The behavior of A_p at low α_N with increasing n is reasonable, because the fluid converges to the Newtonian limit as n approaches unity. Additionally, Fig. 8(b) indicates that the curves of $\Delta\theta_m$ approach the Newtonian curve as n increases. Hence, we may conclude that n is the only parameter shifting the master curves of A_p and $\Delta\theta_m$.

D. Why master curves?: Momentum diffusion versus flow pulsation

The transient dynamics of a flow can be discussed by comparing different time scales of a system [33,34]. Characteristic time defined in Eq. (13), $t_c = \rho H^2/\eta_N$, corresponds to the time for momentum diffusion in the radial direction. Hence, the characteristic viscosity η_N has a direct effect on the time scale over which the flow pulsations propagate in the channel, affecting flow responses. Furthermore, the relationship between the ratio of t_c and the period of the pulsation, $1/\omega$, can be related with Womersley number as

$$\alpha_N^2 = \frac{2\pi f \rho H^2}{\eta_N} = \frac{t_c}{1/\omega}. \tag{39}$$

The numerical data for each case fall on the master curves when plotted against Womersley number, as displayed in Figs. 7 and 8. The result implies that the proposed characteristic viscosity effectively expresses the momentum diffusion over the viscous time scale, t_c, and the Womersley number acts as a dimensionless parameter adequately representing the competition between viscous and pulsatile time scales.

The quasisteady regime occurs at $\alpha_N \ll 1$, where the viscous time scale is small compared to the pulsation time scale. In this low frequency regime, the flow is in phase with the pulsatile mass flow, because the momentum transfer occurs immediately. The inertia-dominant regime can be found at high frequencies when $\alpha_N > 20$, where the period of pulsation is negligible compared to the viscous time scale, so that the flow becomes independent of the pulsation frequency. Here, the amplification factor and phase lag approach unity and $\pi/2$, respectively.

TABLE III. Fitted parameters of master curves of A_p and $\Delta\theta_m$ with different n values.

	Parameters of A_p						Parameters of $\Delta\theta_m$				
n	L	k_1	c_1	k_2	c_2	b	L	k_1	c_1	k_2	c_2
0.5	0.4269	3.982	1.376	1.636	3.271	0.5019	1.338	2.728	0.2757	0.7890	0.9025
0.6	0.3460	4.028	1.443	1.684	3.467	0.6020	1.322	2.740	0.4936	0.8219	1.007
0.7	0.2634	3.996	1.476	1.748	3.729	0.7018	1.312	2.739	0.6797	0.8453	1.104

E. Predicting pulsatile flow dynamics using master curves

This section provides a descriptive example of how to predict pulsatile flow dynamics using the master curves. As discussed in the previous section, the shape of the master curve is n dependent; therefore, the master curves were constructed for n =0.5, 0.6, and 0.7, respectively. Numerical data were obtained from the datasets with the combination of η_0, λ, and f such that the corresponding α_N values could be distributed as evenly as possible on the logarithmic scale. Hence, A_p and $\Delta\theta_m$ were obtained from the data and fitted as

$$A_p = \frac{L}{1+e^{-k_1 \log \alpha_N + c_1}} + \frac{1-L-b}{1+e^{-k_2 \log \alpha_N + c_2}} + b, \tag{40}$$

where L, k_1, k_2, x_1, x_2, and b are the fitting parameters, and the following relationship holds:

$$\Delta\theta_m = \frac{L}{1+e^{-k_1 \log \alpha_N + c_1}} + \frac{\pi/2-L}{1+e^{-k_2 \log \alpha_N + c_2}}, \tag{41}$$

where L, k_1, k_2, x_1, and x_2 are the fitting parameters. Notably, A_p converges to unity as $\alpha_N \to \infty$, and $\Delta\theta_m$ converges to zero as $\alpha_N \to 0$ and to $\pi/2$ as $\alpha_N \to \infty$. These limiting behaviors were exploited to formulate Eqs. (40) and (41). The values of the fitted parameters are listed in Table III, and the constructed master curves are shown in Fig. 9.

To test the accuracy of the fitted master curves, we prepared test datasets that were not used for curve fitting. Three new datasets with different n values (n =0.5, 0.6, and 0.7) were selected, as listed in Table IV. The parameters were selected such that the values of α_N spanned a wide range. For the first dataset with $\alpha_N = 8.587$, the fitted master curve for $n = 0.5$ predicted $A_p = 0.7872$ and $\Delta\theta_m = 1.091$, whereas the computed data yielded $A_p = 0.7854$ and $\Delta\theta_m = 1.095$. The two results are essentially indistinguishable because the differences are below 0.5%, which indicates that our fitted master curve can precisely predict the pulsatile flow behavior. The differences between the

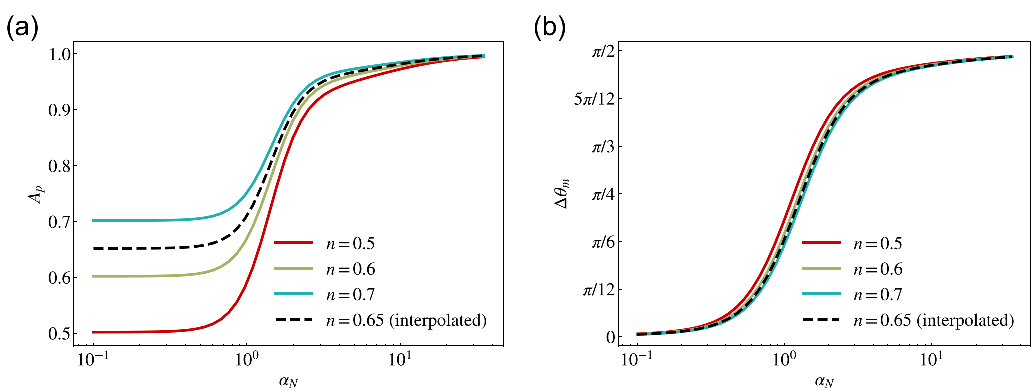

FIG. 9. Fitted master curves of A_p and $\Delta\theta_m$ with different n values ($n = 0.5$, 0.6, and 0.7). The curves for $n = 0.65$ are constructed through the linear interpolation of parameters.

TABLE IV. Carreau parameters, characteristic viscosity, frequency, and non-Newtonian Womersley number of test sets.

Test set	Carreau parameters						
	η_0 (Pa s)	η_∞ (Pa s)	λ (s)	n	η_N (Pa s)	f (Hz)	α_N
1	60	0.01	0.8	0.5	8.587	4	1.656
2	30	0.01	50	0.6	1.227	90	20.78
3	120	0.01	2	0.7	28.59	0.5	0.3209

predicted and computed values for the second and third datasets with different n values are also negligible. The detailed data of the fitted master curves and predicted parameters can be found in the Supplemental Material [32].

We further investigated the practical question of whether the pulsatile flow dynamics of shear-thinning fluids can be predicted with any n value (that is, not only for n =0.5, 0.6, or 0.7). This is demonstrated by the linear interpolation of the curve parameters with respect to n. The interpolated master curves for $n = 0.65$, which seem to be reasonably constructed, are shown in Fig. 9. To test the accuracy, the numerical solution of the pulsatile Carreau flow with $\eta_0 = 50$, $\eta_\infty = 0.01$, $\lambda = 0.1$, $n = 0.65$, and $f = 5$ was used, and A_p and $\Delta\theta_m$ were compared to those estimated based on the interpolated master curve. The differences were 0.18 and 0.063%, respectively, which indicates the remarkable accuracy of the interpolated master curve in terms of predicting the time-dependent flow dynamics. The detailed data are presented in the Supplemental Material [32].

In summary, the proposed approach allows the precise prediction of the pulsatile flow characteristics without explicit transient computations. We emphasize that A_p and $\Delta\theta_m$ can be solely determined by α_N through *steady-state analysis*.

V. FINAL REMARKS

In this paper, we investigated the pulsatile behavior of shear-thinning Carreau fluids based on the Womersley number α_N, which was defined with a reasonable steady-state characteristic viscosity. The numerical experiments conducted in this paper revealed the existence of master curves that exhibit the dependency of A_p and $\Delta\theta_m$ on α_N, and the shape of the master curves was determined by the degree of shear thinning, n. The results imply that the competition between viscous momentum diffusion and flow pulsation can be observed by comparing time scales using the non-Newtonian Womersley number proposed in this paper.

Here, we focused only on the linear transient response regime, where pulsations are sufficiently small ($\approx$10%) such that the pulsatile pressure gradient is solely characterized by the amplitude and phase lag. Notably, A_p and $\Delta\theta_m$ represent the amplitude and phase lag of a shear-thinning flow, respectively, considering that the Newtonian amplitude and phase lag are obtained analytically [10]. The existence of a master curve indicates that the time-dependent characteristics of a shear-thinning pulsatile channel flow can be predicted concisely without fully transient computations. The master curves of A_p and $\Delta\theta_m$ are expressed as parametric equations, and a simple linear interpolation of the curve parameters can reasonably generate the master curves for any n with high accuracy. The proposed approach for predicting time-dependent responses only requires the rheological properties of the fluid, including n, frequency of interest, and steady-state characteristic viscosity.

The scope of this paper was limited to two-dimensional channel flows. However, the proposed approach is expected to be extended to three-dimensional pipe systems using the same methodology. In addition to Carreau fluids, other generalized Newtonian fluids, such as power-law, Cross, and Carreau-Yasuda fluids, can also be analyzed within the same framework. In this paper, the shear-thinning fluid was assumed to be homogeneous; however, complex fluids, such as battery slurries, may exhibit thixotropic behavior owing to changes in their microstructure. Therefore, the proposed approach can be further improved by considering nonhomogeneity.

ACKNOWLEDGMENTS

This work was supported by National Research Foundation of Korea grants funded by the Korea Government (Ministry of Science and ICT) (Grants No. NRF-2018R1A5A1024127, No. NRF-2020R1A2C2008141, and No. NRF-2021M3H4A6A01041234).

---

[1] T. Tsuda, Dynamic response analysis and control of slot coating, J. Fluid Sci. Tech. **4**, 735 (2009).

[2] D. V. Boger, Rheology of slurries and environmental impacts in the mining industry, Annu. Rev. Chem. Biomol. Eng. **4**, 239 (2013).

[3] C. Tao, B. G. Kutchko, E. Rosenbaum, and M. Massoudi, A review of rheological modeling of cement slurry in oil well applications, Energies **13**, 570 (2020).

[4] S. Lanceros-Méndez and C. M. Costa, *Printed Batteries: Materials, Technologies and Applications* (Wiley, New York, 2018).

[5] N. J. Balmforth, I. A. Frigaard, and G. Ovarlez, Yielding to stress: Recent developments in viscoplastic fluid mechanics, Annu. Rev. Fluid Mech. **46**, 121 (2014).

[6] J. Mewis and N. J. Wagner, Thixotropy, Adv. Colloid Interface Sci. **147-148**, 214 (2009).

[7] S. Uchida, The pulsating viscous flow superposed on the steady laminar motion of incompressible fluid in a circular pipe, Z. Angew. Math. Mech. **7**, 403 (1956).

[8] S. Ray, B. Ünsal, F. Durst, Ö. Ertunc, and O. A. Bayoumi, Mass flow rate controlled fully developed laminar pulsating pipe flows, J. Fluids Eng. **127**, 405 (2005).

[9] J. Majdalani, Exact Navier-Stokes solution for the pulsatory viscous channel flow with arbitrary pressure gradient, J. Propul. Power **24**, 1412 (2008).

[10] K. Haddad, Ö. Ertunç, M. Mishra, and A. Delgado, Pulsating laminar fully developed channel and pipe flows, Phys. Rev. E **81**, 016303 (2010).

[11] C. Tu and M. Deville, Pulsatile flow of non-Newtonian fluids through arterial stenoses, J. Biomech. **29**, 899 (1996).

[12] J. Chen and X.-Y. Lu, Numerical investigation of the non-Newtonian pulsatile blood flow in a bifurcation model with a non-planar branch, J. Biomech. **39**, 818 (2006).

[13] J. Boyd, J. M. Buick, and S. Green, Analysis of the casson and carreau-yasuda non-newtonian blood models in steady and oscillatory flows using the lattice boltzmann method, Phys. Fluids **19**, 093103 (2007).

[14] S. Tabakova, N. Kutev, and St. Radev, Oscillatory carreau flows in straight channels, R. Soc. Open Sci. **7**, 191305 (2020).

[15] H. A. Barnes, P. Townsend, and K. Walters, On pulsatile flow of non-newtonian liquids, Rheol. Acta **10**, 517 (1971).

[16] M. F. Edwards, D. A. Nellist, and W. L. Wilkinson, Pulsating flow on non-newtonian fluids in pipes, Chem. Eng. Sci. **27**, 545 (1972).

[17] J. M. DaVies, S. Bhumiratana, and R. B. Bird, Elastic and inertial effects in pulsatile flow of polymeric liquids in circular tubes, J. Non-Newtonian Fluid Mech. **3**, 237 (1978).

[18] N. S. Deshpande and M. Barigou, Vibrational flow of non-newtonian fluids, Chem. Eng. Sci. **56**, 3845 (2001).

[19] E. E. Herrera-Valencia, M. L. Sanchez-Villavicencio, L. Medina-Torres, D. M. Nuñez Ramirez, V. J.ús Hernández-Abad, F. Calderas, and O. Manero, New simple analytical method for flow enhancement predictions of pulsatile flow of a structured fluid, Phys. Fluids **31**, 063104 (2019).

[20] C. W. Macosko, *Rheology: Principles, Measurements, and Applications* (Wiley, New York, 1994).

[21] T. Sochi, Analytical solutions for the flow of carreau and cross fluids in circular pipes and thin slits, Rheol. Acta **54**, 745 (2015).

[22] S. K. Kim, Flow-rate based method for velocity of fully developed laminar flow in tubes, J. Rheol. **62**, 1397 (2018).

[23] J. R. Womersley, Method for the calculation of velocity, rate of flow and viscous drag in arteries when the pressure gradient is known, J. Physiol. **127**, 553 (1955).

[24] M. Ö. Çarpinlioğlu, An overview on pulsatile flow dynamics, J. Thermal Eng. **1**, 496 (2015).

[25] A. Logg, K.-A. Mardal, and G. N. Wells, *Automated Solution of Differential Equations by the Finite Element Method* (Springer, New York, 2012).

[26] H. P. Langtangen and A. Logg, *Solving PDEs in Python* (Springer, New York, 2017).

[27] J. A. Lee, J. Nam, and M. Pasquali, A new stabilization of adaptive step trapezoid rule based on finite difference interrupts, SIAM J. Sci. Comput. **37**, A725 (2015).

[28] R. H. Gallagher, O. C. Zienkiewicz, and J. T. Oden, in *Finite Elements in Fluids* (Wiley, New York, 1982), Vol. 4, pp. 305–318.

[29] E. B. Becker, J. T. Oden, and G. F. Carey, *Finite Elements: Mathematical Aspects* (Prentice-Hall, Englewood Cliffs, NJ, 1983), Vol. 4.

[30] J. N. Reddy and D. K. Gartling, *The Finite Element Method in Heat Transfer and Fluid Dynamics*, 3rd ed. (CRC Press, Boca Raton, FL, 2010).

[31] O. J. Lobo and D. Chatterjee, Development of flow in a square mini-channel: Effect of flow oscillation, Phys. Fluids **30**, 042003 (2018).

[32] See Supplemental Material at http://link.aps.org/supplemental/10.1103/PhysRevFluids.7.123301 for the validation of the numerical method and fitting of the master curves.

[33] A. Yeckel and J. J. Derby, Dynamics of three-dimensional convection in microgravity crystal growth: g-jitter with steady magnetic fields, J. Cryst. Growth **263**, 40 (2004).

[34] O. J. Romero and M. S. Carvalho, Response of slot coating flows to periodic disturbances, Chem. Eng. Sci. **63**, 2161 (2008).